Proceedings of the 5th International Conference on Advanced Science & Engineering ICOASE 2025, University of Zakho and Duhok Polytechnic University, 24th – 25th September 2025

(Special issue for Passer Journal of Basic and Applied Sciences)
Paper No. 01

Synthesis Of Monometallic (Ni) And Bimetallic (Mn–Ni) Nanoparticles Using Vigna Unguiculata Extract for The Adsorption of Congo Red Dye

Lawand L. Mustafa [1], Amin K. Qasim [2]

[1] Technical College of Zakho, Duhok Polytechnic University, Zakho 42002, Kurdistan Region, Iraq.
[2] *College of Science, University of Zakho, Zakho 42002*, Kurdistan Region, Iraq.
Email: lawand.luqman@dpu.edu.krd and amin.qasim@uoz.edu.krd

Abstract

The green synthesis process for Ni and Mn–Ni bimetallic nanoparticles by using Vigna unguiculata seed extract have been investigated for the Congo Red dye adsorption. The aim of the study is to prepare these nanoparticles in more eco-friendly conditions and examine their performance for dye removal from aqueous medium.The plant Vigna unguiculata was selected due to its already proved richness with natural reducing as well as stabilizing agents, especially it is containing of phenolic compounds, flavonoids, and some other bioactive metabolites. These substances have been mentioned in several previous studies for their helping role in formation of nanoparticles, mainly through redox reactions and providing surface passivations. The synthesis was resulted in formation of good-crystallized nanoparticles, with average size about 30 nm for Ni and 22 nm for Mn–Ni particles. The prepared bimetallic Mn–Ni nanoparticles was achieved 83% of dye removal efficiency, which is comparing with 57% for only Ni, giving about 26% enhancement in adsorption activity. The optimum condition was found at 25°C, dye concentration 8 $mg \cdot L^{-1}$, catalyst amount 0.005 g, neutral pH 7, and contact time of 60 minutes. These findings indicate that the bimetallic nanoparticles is having higher adsorption capacity under suitable experimental conditions.Whereas equilibrium data fits the Freundlich isotherm, kinetic analysis verified pseudo-second-order behavior. With (ΔH, ΔS, and ΔG) all negative thermodynamic parameters, the adsorption process was spontaneous and exothermic. While Ni nanoparticles showed greatly decreased reusability, with only 13% efficiency in the third cycle, Mn–Ni nanoparticles retained 51% of their adsorption efficiency after the third reuse cycle. Mn-Ni nanoparticles have a mean zeta potential of -33.8 mV, indicating strong negative surface charge and colloidal stability. These results support the feasibility of Vigna unguiculata-mediated synthesis as an environmentally friendly and reasonably priced technique for manufacturing recyclable adsorbents in wastewater treatment.

Keywords: Mono metallic Ni nanoparticles, Bimetallic Mn-Ni Nanoparticles, Vigna Unguiculata seed Extract, Congo Red Dye, Green Synthesis.

1 Introduction

The globally emissions which are reported from textile industry effluents are still considered very high. It has been pointed out that around 7×10^5 tons of dyes are used annually, and if even around 10% from this amount is released into environment, it may cause serious harmful effects on aquatic life and also other living organisms [1]. The pollution coming from agricultural activities also contributes significantly by producing dangerous chemicals and wastes which are usually not treated properly, like dyestuffs, herbicides, insecticides, and some laboratory effluents. Furthermore, the management of wastewater become more complicated due to increasing contribution of various industrial sources. These include textile factories, agricultural operations, and other anthropogenic activities, which are posing major challenges to treatment process of industrial effluents and control of environmental contamination. [2]. Congo Red, also known as C.I. 22120, is an anionic acidic diazo dye that poses significant health risks to humans. High concentrations of this dye can lead to various diseases, some of which may be fatal. Its cytotoxic properties include genotoxic, hemotoxic, and neurotoxic effects, along with its potential to be carcinogenic and mutagenic[3]. Therefore, Congo Red's complex aromatic structure and sulfonic acid groups allow it to persist in aquatic environments for decades and resist traditional breakdown processes [4].

Adsorption-based techniques are widely recognized in various dye treatment procedures. Recent studies in wastewater treatment have concentrated on adsorbent materials that prioritize sustainability, rapid adsorption rates, cost-

effectiveness, and improved adsorptive performance [5]. Adsorption remains the most widely adopted dye removal technique because of its operational simplicity and scalability[6]. Extensive amount of studies was reported in previous literatures concerning the removal of dyes, which is due to the wide range of adsorbent materials and the relative ease in the operation process. Many types of investigations carried out by using various adsorbents such as activated carbon, activated carbon obtained from biomass sources, carbon nanotube, metal-organic framework, synthetic types of adsorbents, nano-particles, and also other different materials[1].

In recent years, metallic nanoparticles (NPs) have gained prominence as advanced adsorbents, leveraging their high surface area-to-volume ratios and tunable surface chemistries. Despite their efficacy, traditional NP synthesis routes relying on toxic reducing agents (e.g., Sodium Boro hydrate) and stabilizing chemicals contradict sustainability goals by generating secondary pollution [7], [8]. This paradox underscores the necessity of developing eco-friendly synthesis protocols that reconcile nanomaterial efficiency with environmental safety [9]. Sustainable nanoparticle synthesis methods have recently garnered attention for their applications in environmental remediation, especially in water treatment. The ecological compatibility, simplicity, and cost-effectiveness of plant extract-based synthesis methods make them an appropriate alternative for the synthesis of efficient adsorbents. [10]. The bioactive compounds in *Vigna unguiculata* (cowpea) extract have been proven to reduce and stabilize nanoparticle production [11]. Metallic nanoparticles have unique properties, characteristics including diminutive dimensions, extensive surface area, and several active areas. These attributes provide various practical uses, particularly in wastewater treatment for the effective removal of organic contaminants within a shortened contact time [10]. The bimetallic nanoparticles, which are formed from two different kinds of metals, have showed more enhanced characteristics than the single-metal nanoparticles. The combination and distribution of these metals within the nanoparticle structure playing an important role for determining their physical and chemical behaviors. Also, the type of metals used, along with their ratios and concentrations, are affecting the final structure and performance of the bimetallic systems. These factors are together contributing for the improvement in particle's homogeneity and having influence on several macroscopic property like optical absorbance, catalytical activity, and also antibacterial effect. Because of such advantages, the bimetallic nanoparticles are gaining more attentions in recent application of nanotechnology field[12].

Vigna unguiculata, widely cultivated in Kurdistan Region / Iraq for its agricultural significance, was chosen as a sustainable bioresource owing to its high local availability, low cost, and abundance of natural reducing and stabilising agents, including polyphenols and flavonoids[13]. Congo Red is utilized not only in the textile and paper industries but also extensively in higher education laboratories and research institutions as a model dye for studies on adsorption, catalysis, and wastewater treatment. In Iraq, similar to numerous developing nations, laboratory effluents are frequently released into municipal or aquatic environments without adequate treatment, which may lead to localized contamination. The persistence, high solubility, and potential toxicity of Congo Red to aquatic organisms render it an appropriate and environmentally significant model pollutant for assessing the efficacy of green-synthesized adsorbents.

While photocatalytic degradation is widely explored for pollutant removal, however, adsorption is frequently favored in practical wastewater treatment because of its operational simplicity, cost-effectiveness, and efficiency at low contaminant concentrations. In this study, Mn monometallic nanoparticles were not synthesized, as the primary objective was to assess the adsorption performance enhancement achieved by incorporating Mn into a Ni-based bimetallic system, in comparison with monometallic Ni nanoparticles synthesized under the same green conditions. This study selected Mn–Ni bimetallic nanoparticles due to their unique compositional synergy; manganese enhances surface reactivity, whereas nickel improves structural integrity. While Mn–Ni systems have been studied for catalytic and electrochemical applications, their potential as adsorbents, particularly when synthesized through green methods, has not been thoroughly examined. This research is concentrated on the development of eco-friendly as well as novel method for the synthesis of monometallic Ni nanoparticle and also bimetallic Mn–Ni nanoparticles by utilizing the extract from Vigna unguiculata seeds, which it serves as both reducing agent and also stabilizer. The method is aiming to provide green alternative towards conventional synthesis approaches, and the plant-based extract is playing important role in the formation and controlling of the nanoparticle's properties. The adsorption efficiency of these prepared nanoparticles was studied in detail for removal of Congo Red dye from aqueous solution under various physicochemical parameters such as temperature, pH values, dosage amount and contact times. The mechanism of adsorption process have been analysed through applying kinetic, isotherm, and also thermodynamic models in order to understand the behaviour and interaction. Moreover, the possibility of reusing the nanomaterials and improvement in adsorption performance due to bimetallic structure also were investigated and discussed.

2 Material and Methods

2. 1 Materials

Fresh seeds of Vigna Unguiculata (Cowpea) were procured from Chamke Delal, Zakho, Kurdistan Region, Iraq. The scientific classification is Vigna Unguiculate, a member of the Fabaceae family. All chemicals used were of analytical grade. Manganese nitrate tetrahydrate [$Mn(NO_3)_2 \cdot 4H_2O$] was obtained from Sigma-Aldrich (St. Louis, MO, USA; EMSURE grade) purity ≥98.5%, and nickel nitrate hexahydrate [$Ni(NO_3)_2 \cdot 6H_2O$] was purchased from CARLO ERBA Reagents (Val de Reuil, France) purity ≥99 %. Congo Red dye, sodium hydroxide (NaOH, 97%), and hydrochloric acid (HCl, 37%) were supplied by Merck (Darmstadt, Germany).

2. 2 Phytochemical Screening

The Vigna unguiculata (Cowpea) seed extract underwent phytochemical studies following standard methods [13], [14].

2. 3 Preparation of the Cowpea seed extract

Fresh seeds were harvested, thereafter dried in the shade at room temperature for 15 days, and then ground using an electric grinder[13] . Subsequently, for the monometallic nickel nanoparticles green synthesis and bimetallic Manganese-Nickel nanoparticles, 10 g of powder was dissolved in 100 mL of deionized water in a 250 mL conical flask, followed by heating at 65°C for 45 min while stirring continuously. Subsequently, filtration was performed, and the filtrate was centrifuged at 7000 rpm for 15 min to obtain a pure aqueous extract. These phytochemicals not only act as reducing agents facilitating the conversion of metal ions to nanoparticles, but also function as stabilizing and capping agents, which help prevent nanoparticle agglomeration and influence their morphology and size distribution.

2. 4 Synthesis of monometallic Ni nanoparticles

For the synthesis of Ni NPs. 100 mL of 0.01 M of $Ni(NO_3)_2.6H_2O$ was prepared in DI water. The solution was kept under continuous stirring at 650 rpm. Then, 30 mL from extract added drop-by-drop into the solution containing nickel nitrate while stirring to ensure proper mixing. After that, 1 M of sodium hydroxide (NaOH) was added gradually for adjusting the pH of solution to 12 while continuing the stirring. The reaction mixture was kept on magnetic stirrer at 70 °C for 60 minutes. After that, the observation of the color change, which indicate the formation of nickel nanoparticles. The solution was centrifuged at 10,000 rpm for 10 minutes in order to collect the synthesized nanoparticles. The collected particles were washed several times with deionized water and one time by ethanol, and then dried in oven at 45 °C for 24 hours. The successful synthesis of Ni NPs was confirmed through UV-Vis spectroscopy measurement.

2. 5 Synthesis of bimetallic Mn-Ni nanoparticles

For bimetallic Mn-Ni NPs synthesis, 100 mL of 1:1 0.01 M of $Mn(NO_3)_2.4H_2O$ Manganese Nitrate tetrahydrate with 0.01M $Ni(NO_3)_2.6H_2O$ nickel nitrate hexahydrate was prepared in DI water. 30 mL of seed extract added drop by drop to the solution. Adding 1 M NaOH to adjust the pH at 12 with stirring continuously. The solution was kept on the stirrer at 70°C for 120 min with exact washing, drying procedure same as synthesized Ni NPs.

2. 6 Characterization

The crystallinity was evaluated using powder X-ray diffraction (PXRD) with a D8-advanced diffractometer (Haoyuan Instrument Co. Ltd, DX-2700BH) over a scan range of θ 5-80°. Energy-dispersive X-ray spectrometry (EDS) mapping was employed for elemental analysis (Quanta 4500, Germany). Field emission scanning electron microscopy (FE-SEM, ZEISS, SIGMA VP, Germany) was employed to examine the morphology of the synthesized microspheres. Fourier transform infrared (FTIR) spectra were acquired utilizing a Perkin Elmer Spectrum Two within the range of 450 to 4000 cm^{-1}. Absorbance spectra were obtained using a JENWAY 6700 and a Perkin-Elmer Lambda 25, USA, employing a 1 cm path length cell. Zeta potential of particles using the iontophoresis laser doppler method was measured by Horiba SZ-100.

2. 7 Batch adsorption experiments

To evaluate the effectiveness of synthesized nanoparticles in the removal of Congo red dye from aqueous solutions, comparative research was performed. Batch experiment was carried out in order to examine the influence of different variable conditions on the studied system, where each factor was tested separately under controlled manner to observe its specific effect, including initial dye concentration range of (2 to 10 mg.L^{-1}), pH (6.5, 7, 7.5, 8, 10), contact time (2–64 min), temperature (15, 20, 25, 30 and 35 °C), and adsorb the absorbance measured and checked for the supernatant. The adsorption capacity q_e was calculated then afterwards according with following formula. [15]:

$$q_e = \frac{(C_0 - C_e) * V}{m} \qquad (1)$$

where

q_e = adsorption capacity

C_o = initial concentration

C_e = equilibrium concentration

V = solution volume in Liter

m = adsorbent mass in grams

The adsorption efficiency can be quantified by determining the percentage removal of dye as follows:[16], [17]:

$$\%\ Dye\ Removal = \frac{(C_i - C_e)}{C_i} \times 100 \qquad (2)$$

where

C_i = initial concentration

C_e = equilibrium concentration

Freundlich model and Langmuir model isotherms were utilized for the equilibrium experimental data. The Langmuir is expressed by the equation [16]:

$$\frac{C_e}{q_e} = \frac{1}{bq_{max}} + \frac{1}{q_{max}} C_e \qquad (3)$$

where

C_e = equilibrium concentration of dyes solution

q_e = adsorbate solid-phase concentration at equilibrium

q_{max} = adsorption capacity at maximum

b = Langmuir constant

The intercept value of $1/bq_{max}$ is determined with the graph of C_e/q_e vs C_e. R_L the dimensionless factor, often known as the separation factor, is an additional distinguishing parameter of the Langmuir isotherm, as articulated in the equation [15]:

$$R_L = \frac{1}{(1 + bC_o)} \qquad (4)$$

where R_L= dimensionless factor

C_o = the greatest dye concentration

b = Langmuir constant

The value of *R*L is contingent upon the isotherm type and may indicate adverse conditions ($R_L > 1$), linear ($R_L = 1$), favorable ($0 < R_L < 1$), or irreversible ($R_L = 0$) adsorption [18]. The Freundlich isotherm is being an empirical expression which describe the sorption process occurred on heterogeneous surfaces, or on those surfaces that they have different affinity sites. The logarithmic form for the Freundlich equation can be written as follow:

$$lnq_e = lnK_f + \frac{1}{n}\ lnC_e \qquad (5)$$

where K_f= the adsorption capacity

n = intensity

K_f is a constant that represents the efficiency of adsorption. The slope of 1/n, ranging from 0 to 1, serves as an indicator of adsorption intensity or surface heterogeneity, with increased heterogeneity observed as the slope approaches zero. A ratio of 1/n less than 1 indicates a conventional Langmuir isotherm, while a value of 1/n greater than 1 signifies cooperative adsorption. K_f and n can be calculated from plotting lnq_e vs. lnC_e. The kinetics of adsorption were examined using pseudo first order and pseudo second order models. Pseudo First order is expressed by the Lagergren equation, which calculates the adsorption rate constant (k_1) from the graph of $\ln(q_e - q_t)$ versus t, where q_e and q_t denote the adsorbed amount at equilibrium and at time t, respectively [19].

$$\ln(q_e - q_t) = \ln q_e - k_1 t \qquad (6)$$

where

q_e = adsorbed amount at equilibrium

q_t = adsorbed amount at time t

The (pseudo second-order) model, conversely, determines the second order rate constant (k_2) from the linear graph of t/qt versus t.

$$\frac{t}{q_t} = \frac{1}{k_2 q_e^2} + \frac{1}{q_e}\ t \qquad (7)$$

The (ΔG°), (ΔH°), (ΔS°) thermodynamic parameters, were calculated using the following equations that incorporate the equilibrium constant (K_c), absolute temperature (T), and the universal gas constant (R). The $\Delta H°$ value and $\Delta S°$ value can be calculated from the Van't Hoff equation, the parameters were derived using the ln Kc against 1/T plot, where the slope indicates $-\Delta H^\circ/R$ and the intercept signifies $\Delta S^\circ/R$ [17].

$$lnK_c = \frac{\Delta H^\circ}{RT} + \frac{\Delta S^\circ}{R} \qquad (8)$$

$$\Delta G^\circ = -RTlnK_c \qquad (9)$$

$$K_c = \frac{q_e}{C_e} \qquad (10)$$

The capacity of an adsorbent to be regenerated and reused with optimal adsorption effectiveness is a crucial characteristic for effective adsorption applications. To evaluate the feasibility of renewing Mn: Ni nanoparticles were combined with 5 ml of Congo Red dye at a concentration of 8 $mg.L^{-1}$ and 0.005 g of Mn. Ni nanoparticles were placed on shaker for 60 min at a temperature of 25 °C and a pH of 7.0, with the concentration of adsorbed dye measured using a UV-Vis spectroscopy instrument. The adsorbent was regenerated by washing it with a 50% ethanol (v/v) solution in deionized water, with the regeneration procedure repeated for two cycles. The dye concentration in the ethanol solution was evaluated using a UV-Vis spectrophotometer. The adsorption-desorption procedure was

conducted for two cycles. The regeneration percentage (Re%) was calculated using an equation as shown in equation 11 [20].

$$\% R = \frac{V.C_m}{M.q_e} \times 100 \qquad (11)$$

3 Result and Discussion

3. 1 Phytochemical Screening

The principal distribution of *Vigna unguiculata* (Cowpea) is in India, Central America, China, and Africa. *Vigna unguiculata*. The presence of flavonoids, alkaloid, glycoside and phenolic compounds in the cowpea extract suggests their active role in nanoparticle synthesis. These bioactive molecules are known to facilitate the reduction of metal ions to nanoparticles and simultaneously act as capping and stabilizing agents, influencing the size, shape, and dispersion stability of the synthesized Ni and Mn–Ni nanoparticles. The results of phytochemical screening of Vigna unguiculate (Cowpea) plant are shown in **Figure 1** & **Table 1**.

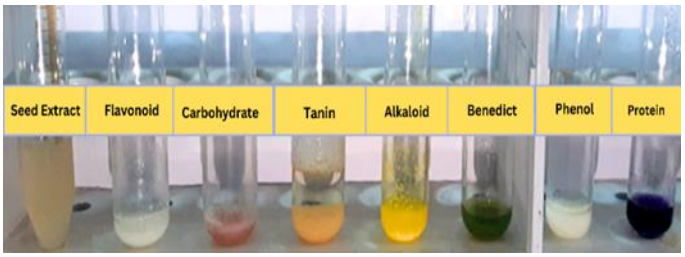

Figure 1: *The phytochemical Screening test results for cowpea seed extract.*

Table 1: Phytochemical analysis of Vigna unguiculata seed extract.

Active constituent	Results	Chemical test
Glycoside	Positive	Benedict
Tannin	Negative	Braymer
Flavonoid	Positive	Lead acetate
Carbohydrate	Positive	Molish
Alkaloid	Highly Positive	Hager
Phenolic	Highly Positive	Lead acetate
Proteins & A.acid	Positive	Ninhydrin
Saponin	Highly Positive	Foam

3. 2 FE-SEM Analysis

The FE-SEM image in **Figure 2 (a)** and **(b)** with scale of 500 nm illustrate the unique morphological characteristics of Ni and Mn-Ni nanoparticles, which are essential for their use for the Congo Red dye adsorption. The Ni NPs **in Figure 2 (a)** manifest as irregular aggregates, but the Mn-Ni nanoparticles in **Figure 2 (b)** exhibit more uniform, spherical forms, indicating enhanced particle distribution attributed to the inclusion of manganese. The particle size distribution histograms reveal an average size of roughly 22 nm for the Mn-Ni nanoparticles, which is lower than that of the pure Ni particles 30 nm. The diminished particle size is advantageous for adsorption operations, since smaller particles often provide an increased surface area, hence improving the interaction between the nanoparticles and the Congo Red dye molecules. The enhanced dispersion of Mn-Ni nanoparticles may contribute to the prevention of aggregation, hence augmenting their adsorption efficacy. The structural and dimensional alterations of Mn-Ni nanoparticles are anticipated to markedly enhance their efficacy in dye removal applications, as they can engage more efficiently with bigger dye molecules, such as Congo Red.

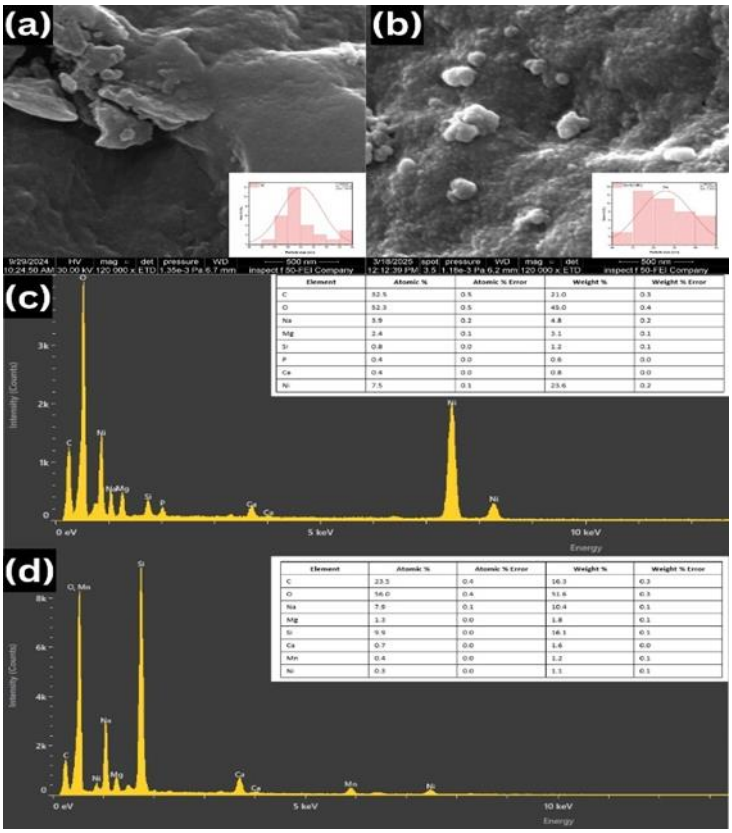

Figure 2: (a, b) FE-SEM image of green synthesized & particle size distribution histogram of (a) Ni NPs, (b) Mn-Ni NPs. (c, d) EDX spectra of (c) Ni NPs (d) Mn-Ni NPs.

3. 3 Energy Dispersive X-ray analysis (EDX)

EDX analysis of Ni and Mn-Ni NPs was performed to confirm their composition and distribution, as depicted in **Figure 2 (c)** and **(d)**, respectively. Distinct peaks for Ni and Mn displayed in EDX spectra, validating the production of Ni and Mn-Ni nanoparticles. The distinct signal peaks display at 0.9 keV, 7.6 keV, and 8.25 keV for Ni in the EDX spectra, signifying the presence of Ni metal, alongside a peak at 5.9 keV and 0.5 keV for Mn[21], [22]. Moreover, the EDX spectra reveal the presence of other elements that may have arisen from contamination during the analysis processes. The EDX spectra clearly displayed peaks for carbon (C) and oxygen (O), confirming the adsorption of biological components onto the nanoparticle surface sourced from the seed extract.

3. 4 Uv-Visible Spectroscopic Analysis

The UV-Vis absorption spectra offer essential information regarding the optical characteristics and electrical interactions that specify the behaviour of the produced nanoparticles. The plant extract displays a specific absorption maximum at 311 nm **Figure 3(a)**, aligning with $\pi \rightarrow \pi^*$ electronic transitions in conjugated aromatic systems typical of phenolic chemicals and flavonoids. This assignment corresponds with Fourier-transform infrared (FTIR) spectroscopic data, which indicate significant O-H stretching vibrations and carbonyl (C=O), thereby affirming the existence of biomolecules that promote metal ion reduction and nanoparticle stabilization. Ni NPs have a red-shifted absorption peak at 338 nm, signifying effective nanoparticle synthesis. This bathochromic shift corresponds with FESEM findings of increased particle size (~30 nm), presumably resulting from agglomeration-induced electron delocalization. Agglomeration diminishes quantum confinement effects, therefore prolonging the wavelength necessary for inter-band transitions. For Mn-Ni NPs, a hypsochromic shift to 322 nm observed compared to Ni NPs, along with a decrease in average particle size to around 22 nm (FESEM). The blue shift is ascribed to charge-transfer transitions at the Mn-Ni interface, where electron density reallocates between the d-orbitals of Mn^{2+} and Ni^{2+}. Such interactions alter the electronic band structure diminishing the wavelength necessary for excitation.

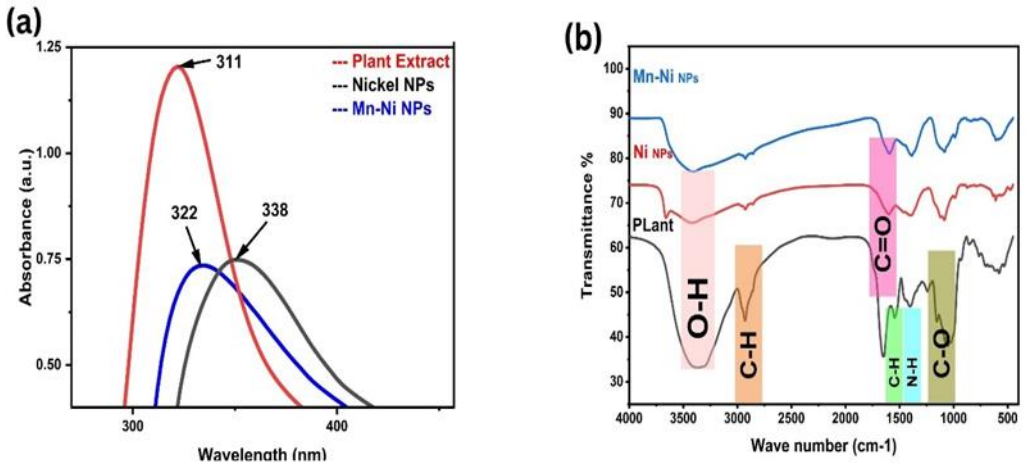

Figure 3: (a) Uv-Visible image of green synthesized, Plant extract, Ni NPs, and Mn-Ni NPs. (b) FTIR spectra of Plant extract, Ni NPs and Mn-Ni NPs.

3. 5 Fourier Transform Infrared Analysis (FTIR)

The FTIR spectroscopy identified the functional groups that's essential in nanoparticle formation and stability. The plant seed extract spectrum exhibits a wide absorption band at 3000–3500 cm^{-1}, attributed to O-H stretching vibrations in phenolic hydroxyl groups, and a unique peak at 1650–1750 cm^{-1}, associated with C=O stretching in carbonyl-containing biomolecules such as flavonoids or proteins **Figure 3 (b)**.

These bands indicate the presence of reducing and capping agents essential for the reduction of metal ions. Upon synthesis, the FTIR spectra of Ni and Mn-Ni nanoparticles display reduced intensities of O-H and C=O peaks, indicating the engagement of ligands in the reduction of metal ions and the stabilization of nanoparticles.

Mn-Ni nanoparticles exhibit residual O-H vibrations, indicating the partial retention of biomolecules on their surface. Comparative research indicates that Mn-Ni nanoparticles display a slightly more pronounced C=O peak than Ni nanoparticles, possibly suggesting a change in biomolecule orientation on the bimetallic surface.

3. 6 XRD Analysis

Crystallographic features of the X-ray diffraction (XRD) patterns for **Figure 4 (a)** Ni NPs and **Figure 4 (b)** Mn-Ni NPs show differences. **Figure 4 (a)** shows different reflections at (111), (200), and (220), in line with the face-centred cubic (FCC) structure of metallic nickel (JCPDS 03-1051)[23], therefore verifying the formation of phase-pure Ni nanoparticles.

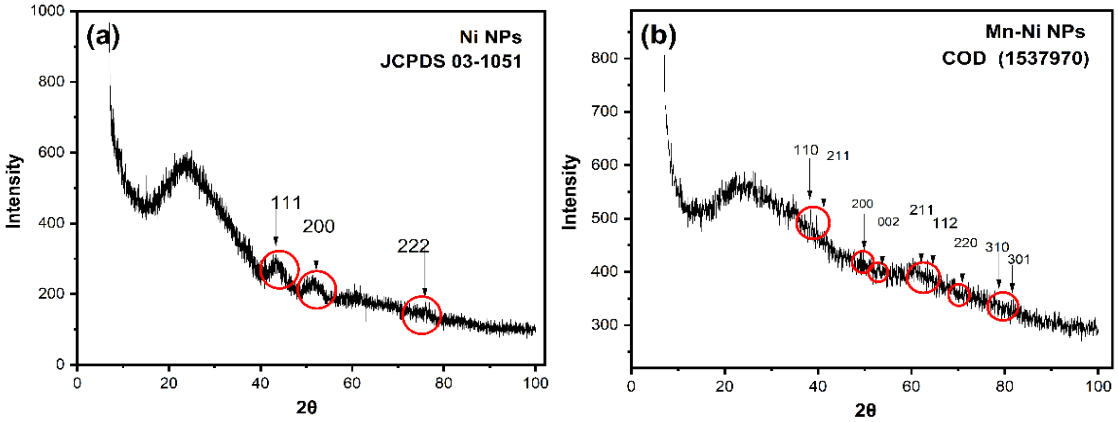

Figure 4: XRD pattern of green synthesized (a) Ni NPs, (b) Mn-Ni NPs.

Figure 4(b) shows a changed profile marked by notable peaks at (211), (200), and (202) as well as secondary reflections at (212) and (312), which imply structural distortion resulting from manganese inclusion. The measured deviations match the $L1_0$ tetragonal phase (COD 15379) [24], in which Mn atoms occupy certain lattice positions resulting in compressive strain and a reduction in symmetry. While Scherrer analysis estimates crystallite sizes of roughly 10.94 nm for Ni nanoparticles and 2.15 nm for Mn-Ni nanoparticles, matching FESEM data, the absence of oxide-related peaks in both samples confirms the predominance of the metallic phase.

With lattice parameters (e.g., a = 3.52 Å for Ni compared to a = 3.73 Å and c = 3.52 Å for Mn, the change from FCC (Ni) to tetragonal symmetry (Mn-Ni) shows effective alloy formation and indicates electronic modulation produced by Mn. The outcomes confirm the synthesis of a bimetallic system with tailored structural features.

The dislocation density, microstrain, and stacking faults were determined using the subsequent equations:

$$(\delta) = \frac{1}{D^2} \qquad (12)$$

$$\varepsilon = \frac{\beta \cos\theta}{4} \qquad (13)$$

$$(S.F) = \left[\frac{2\pi^2}{45(3\tan\theta)\frac{1}{2}}\right]\beta \qquad (14)$$

Table 2: X-ray Diffraction-Based Structural Characterization of Ni and Mn-Ni Nanoparticles

Sample	D(nm)	2θ(°)	Dislocation Density (lines/m²)	Microstrain	Stacking Fault
Ni	10.9	0.016	0.044	7.545	0.016
		0.013	0.039	6.406	0.013
		0.003	0.0211	3.046	0.003
Mn-Ni	2.15	34.02	1	0.339	1.125
		35.05	0.0509	0.0780	0.255
		63.53	0.098	0.107	0.282
		71.63	3.42	0.571	1.456
		81.73	0.16	0.137	0.342
		86.99	0.64	0.262	0.652

As shown in **Table 2**, Mn-Ni nanoparticles exhibit significantly increased dislocation density and microstrain relative to monometallic Ni nanoparticles, signifying greater lattice distortions and defect concentrations due to Mn inclusion. These imperfections contribute to surface activity and reactivity. The decreased dislocation density and microstrain in Ni nanoparticles indicate a more stable and less strained crystalline structure. The density of stacking defects in Mn-Ni nanoparticles is reduced, signifying improved structural ordering relative to nickel nanoparticles. The combination of increased defect density and reduced crystallite size enhances the adsorption capacity of Mn-Ni nanoparticles for Congo Red dye, likely due to synergistic structural and electronic effects arising from the bimetallic composition.

3. 7 Zeta Potential Analysis

The zeta potential of the Mn-Ni bimetallic nanoparticles (-33.8 mV) signifies a strong negative surface charge, as shown in **Figure 5**, implying superior colloidal stability and dispersion. Despite the electrostatic repulsion between the negatively charged nanoparticles and the anionic Congo Red dye, the high adsorption efficiency (83%) indicates that surface functionalization from green synthesis significantly enhances the nanoparticle surface, promoting hydrogen bonding, π-π stacking, and hydrophobic interactions, which remain unaffected by surface charge[25]. The bimetallic synergy between Mn and Ni increases the surface area and reactivity, hence offering additional active sites for dye interaction. Modifications in pH and ionic strength can change the surface charge, potentially enhancing adsorption by neutralizing electrostatic repulsion, while non-electrostatic forces such as van der Waals interactions additionally facilitate successful dye uptake.

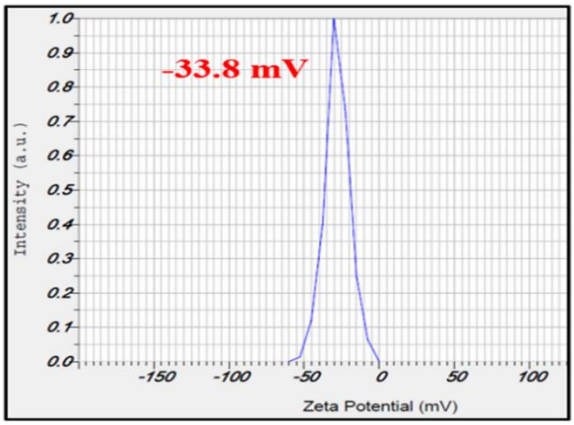

Figure 5: Zeta Potential analysis of Mn-Ni nanoparticles

3. 8 Adsorption Study

Effect of the initial dye concentration**:** Congo Red solution initial concentration effect on the adsorption efficiency was examined at varying levels of 2, 4, 6, 8, and 10 mg L^{-1} using synthesized nanoparticles, while keeping parameters constant according to literature review, including (60 min) time, (25°C) temperature with pH (7.0), and adsorbent dose (0.005 g). As shown in **Figure 6** an increase in relation to the initial concentration of the dye solution observed from the removal percentage. The highest removal efficiency was observed at 8 mgL^{-1}, achieving 70.4% for Mn-Ni and 16% for Ni nanoparticles. As the initial concentration increase, a greater number of Ni and Mn-Ni NPs active sites are surrounded by dye molecules [26], the dye molecules driving forces increased, leading to an enhancement in the sorption process [15], [19]. However, above a specific concentration, no further absorption of dye molecules transpired, signifying that equilibrium was attained. This indicates that the nanoparticle surface reaches complete saturation, leaving no available area for further adsorption [10]. The optimum initial concentration found to be 8$mg.L^{-1}$.

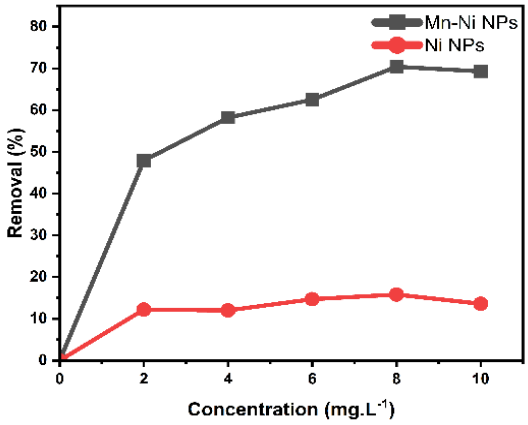

Figure 6: Effect of initial dye concentration on the removal percentage of Congo Red using Ni, Mn-Ni NPs.

Effect of solution pH: The effect of pH on the adsorption of Congo Red dye utilizing Ni and Mn-Ni nanoparticles was investigated to determine the optimal pH level. Congo Red dye serves as a pH indicator, with a blue shift occurring when testing pH levels below 5 [27]. Various solutions of Congo Red were prepared from a stock solution and adjusted to pH levels ranging from 6.5 to 10 [28], under controlled conditions (concentration of 8 mgL^{-1}, duration of 60 min, adsorbent dosage of 0.005 g, and ambient temperature of 25°C). The data presented in the **Figure 7** indicate that increase Congo Red removal with increasing pH, with maximum removal occurring at a pH of 7 for both NPs. The adsorption capacity subsequently declined beyond this pH level[15]. Bimetallic Mn-Ni demonstrated a removal efficiency of 82%, surpassing the 49.2% achieved by monometallic systems. A pH of 7 was chosen for the study to optimize adsorption capacity and elucidate the potential adsorption mechanism.

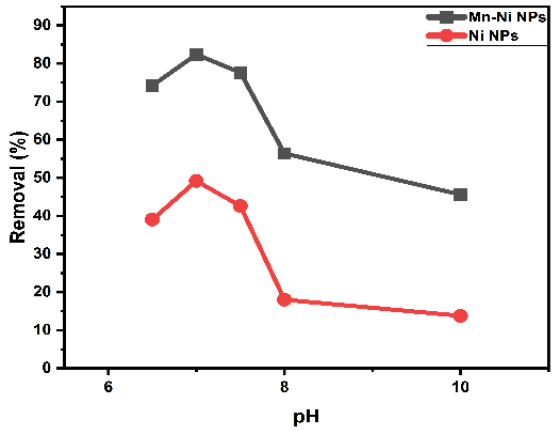

Figure 7: Effect of solution pH on the removal percentage of Congo Red dye using Ni, Mn-Ni NPs.

Effect of Temperature: Under optimum conditions at different temperatures (15, 20, 25, 30, 35 and 40°C) the effect of temperature on the adsorption behaviour of Congo Red dye on to Ni nanoparticles and Mn-Ni nanoparticles was investigated, as illustrated in **Figure 8**, the removal efficiency showed a significant decreasing trend with the increasing of temperature. The maximum percentage of removal for Congo Red was recorded at 25°C, being 57% for Ni NPs and 82% for Mn-Ni NPs, respectively. This reduction at higher temperatures can be explained by the increasing in molecular kinetic energy, which may result in weaken of electrostatic interaction between dye molecules and the adsorbent surface. These observations give indication that the adsorption process of Congo Red in current study is likely exothermic in nature. [10], [29]. 25°C temperature selected for further experimental studies.

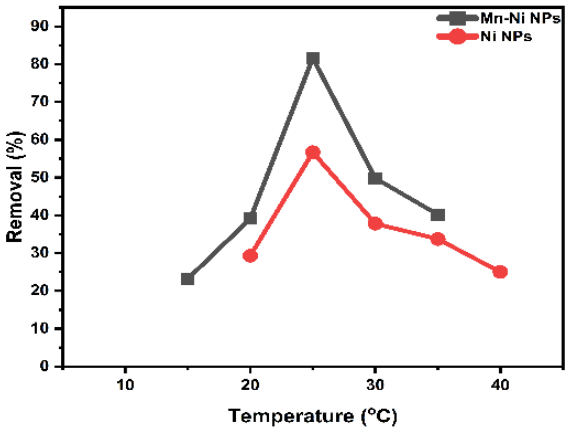

Figure 8: Effect of temperature on the dye removal percentage for Congo Red using Ni, Mn-Ni NPs.

Effect of adsorbent dose: The impact of varying catalytic dosages of Ni and Mn-Ni nanoparticles on adsorption efficiency was examined across four different dosages, ranging from 0.0025 to 0.01 g, while maintaining consistent experimental conditions as previously described. **Figure 9** illustrates that the maximum removal was 57% for Ni NPs and 82% for Mn-Ni NPs at a dosage of 0.005 g. The findings demonstrate that augmenting the dosage of nanoparticles markedly improves the removal effectiveness of Congo Red. The existence of active sites on nanoparticles substantially influences the efficacy of dye elimination. Surpassing the optimal dose of 0.005g leads to a reduction in removal capacity, mainly attributed to agglomeration, which decreases the effective surface area and limits dye accessibility to active sites.

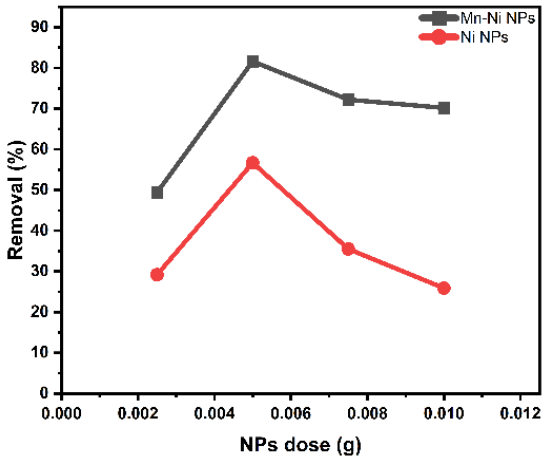

Figure 9: Adsorbent dose effect on the percentage removal of Congo Red dye with Ni, Mn-Ni NPs.

Effect of contact time: The beneficial effect of time on the adsorption of Congo Red dye was analyzed by assessing the removal percentage at various periods of time. The results **Figure 10** indicate that the adsorption process occurred rapidly in the initial stages and decelerated as it approached equilibrium at 60 min[26]. The removal percentages were 57% for Ni nanoparticles and 83% for Mn-Ni nanoparticles, at 8 mg L^{-1} dye concentration. This behavior is attributable to the active surface area availability on Ni and Mn-Ni nanoparticles. As time progresses, the active surface area becomes depleted, resulting in a limited number of vacant surface sites and consequently slowing the adsorption process. The adsorption attains equilibrium after 60 min.

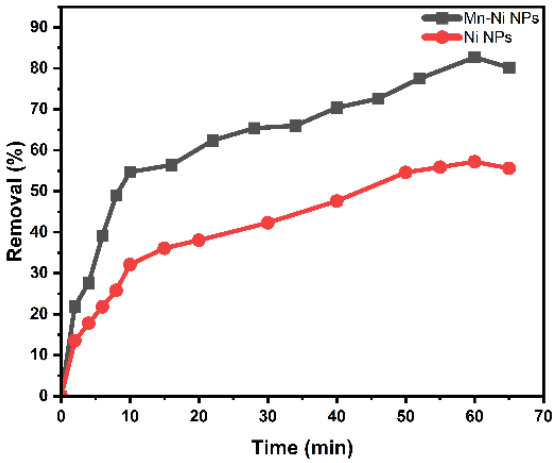

Figure 10: Contact time effect on the removal percentage of Congo Red dye using Ni and Mn-Ni NPs.

As its illustrated in **Table 3** which highlights the optimum conditions for the Adsorption of Congo Red dye using Ni and Mn-Ni NPs.

Table 3: Optimum Condition for Congo Red dye adsorption.

Dye conc.	pH	Temp.	NPs Dose	Contact Time
8 mgL^{-1}	7	25 °C	0.005 g	60 min

3. 9 Adsorption isotherms

In this study, Langmuir model and Freundlich model were selected due to their widespread applicability in dye adsorption studies and their effectiveness in describing monolayer adsorption on homogeneous surfaces and multilayer adsorption on heterogeneous surfaces, respectively, which are relevant to the synthesized nanoparticles. The

adsorption data onto Ni, Mn-Ni nanoparticles aligns with the Freundlich isotherm model, exhibiting high R^2 values in comparison to the Langmuir isotherm, as illustrated in **Table 4** and **Figure 11(a, b)**.

This indicates that the adsorption process is heterogeneous and encompasses multiple adsorption sites. The binding of adsorbate molecules to specific surface sites is believed to occur with greater frequency than to others, due to the non-uniformity of the adsorbent surface. Furthermore, it is conceivable that the adsorbent surface displays a degree of surface heterogeneity, suggesting that the surface energy varies across the adsorbent material[19].

Table 4: Isotherm parameters for the Congo Red dye adsorption onto Ni and Mn-Ni NPs.

NPs	Langmuir				Freundlich		
	q_{max} (mg.g^{-1})	K_L (L.mg^{-1})	R_L	R^2	K_f	1/n	R^2
Ni	-4.9	-0.02	1.26	0.3859	0.116	1.175	0.9691
Mn-Ni	-2.99	-0.24	1.941	0.8625	0.841	1.925	0.9736

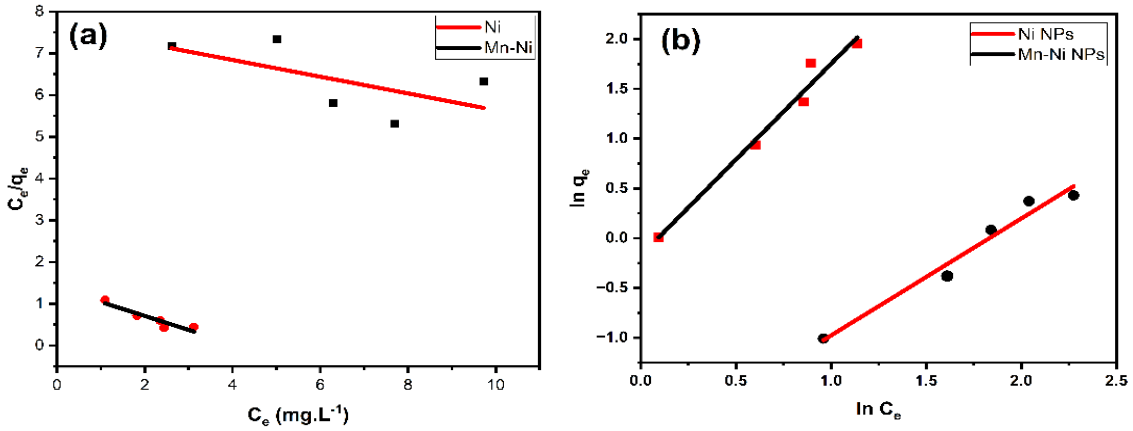

Figure 11: Adsorption isotherms (a) Langmuir (b) Freundlich model.

3. 10 Adsorption kinetic

The adsorption kinetic was studied by applying the pseudo-first order and pseudo-second order kinetic models. The experimental adsorption data were fitted to both models, and the values of correlation coefficients was compared, as it is presented in **Table 5** and **Figure 12** (**a** and **b**). The correlation coefficient which is near to 1 mean the model is more accurate in describing the adsorption mechanism. In this work, the correlation coefficient for pseudo-first-order and pseudo-second-order models were found to be 0.7894 and 0.9903 for Ni NPs, while for Mn-Ni NPs the values was 0.6836 and 0.9909 respectively. The pseudo-second-order model giving higher correlation values in both nanoparticles than the pseudo-first-order, which indicating its better fitting to the adsorption process.

Therefore, the obtained results confirm that the adsorption behaviour of Congo Red dye on the surface of Ni and Mn-Ni nanoparticles follows chemical type of adsorption proces [30] s.

Table 5: Kinetic Parameters for adsorption of Congo Red dye synthesized Ni and Mn-Ni NPs.

NPs	Pseudo-first-order			Pseudo-second-order		
	K_1 (min^{-1})	q_e (mg.g^{-1})	R^2	K_2 (g.mg^{-1}min^{-1})	q_e (mg.g^{-1})	R^2
Ni	1.56024	0.01803	0.7894	5.3246	0.02206	0.9903
Mn-Ni	2.89244	0.0152	0.6836	7.1008	0.01707	0.9909

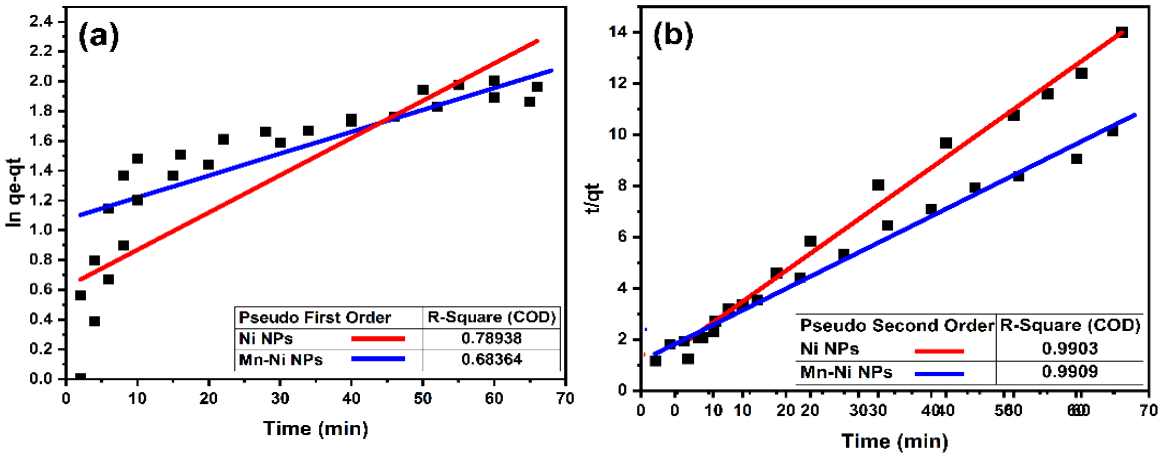

Figure 12: Pseudo (a) first-order and (b) second-order kinetics of adsorption of Congo Red dye onto Ni and Mn-Ni NPs.

3. 11 Thermodynamic Study

Table 6 and **Figure 13** illustrate that the enthalpy change, ΔH, is negative, indicating that the adsorption of Congo Red dye on Ni, Mn-Ni NPs is exothermic. Additionally, the negative value of ΔS signifies a decrease in randomness and a reduced likelihood of accidental contacts between the adsorbent and the solution. The standard (ΔG°) values transition from negative to positive with increasing temperature, signifying a temperature-dependent shift in spontaneity. The process is spontaneous within the temperature range of 25–30 °C and becomes non-spontaneous at temperatures exceeding 35 °C. This pattern aligns with the thermodynamic parameters: a negative enthalpy change (ΔH° = –132.61 kJ/mol) and a negative entropy change (ΔS° = –433.03 J/mol·K). The observed peak spontaneity at approximately 25 °C indicates an optimal operational range, beyond which thermodynamic favorability decreases.

Table 6: Thermodynamic parameters of Congo Red adsorption onto Ni and Mn-Ni NPs.

NPs	ΔH° (kJ/mol)	ΔS°(J/mol K)	ΔG° (kJ/mol)				R^2
			25°C	30°C	35°C	40°C	
Ni	-69	-232	-0.66	0.68	1.72	2.84	0.9968
Mn-Ni	-132	-433	-3.6	-1.10	1.009	2.79	0.9931

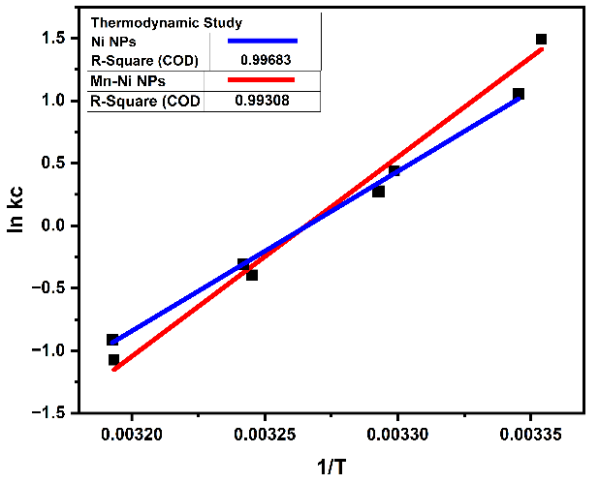

Figure 13: Thermos dynamic study of Congo Red adsorption onto Ni and Mn-Ni NPs.

3. 12 Regeneration results

The regeneration behavior of Ni and Mn-Ni nanoparticles was investigated during three repeated cycles through recycling of the prepared nanoparticles in the Congo Red dye solution. As shown in **Figure 14**, the removal percentage

was observed to be the highest at the first cycle. This obtained result could be explained by the fact that many of the active sites on the adsorbent surface were already occupied with dye molecules after the adsorption process has occurred. Therefore, the number of the available sites become limited in the following cycles, which is causing a clear reduction in the removal efficiency of Congo Red dye.

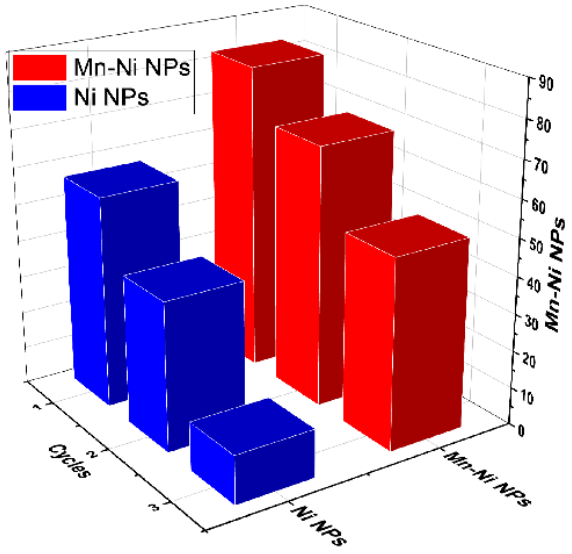

Figure 14: The Recyclability of Ni and Mn-Ni NPs for the removal of Congo Red dye.

As illustrated in **Figure 15 (a)**, depicting the material prior to dye adsorption, nanoparticles display in the range of 10 nm to not more than 35 nm with an averaging of 22 nm in size, predominantly spherical and uniformly distributed. Their polished surface signifies a regulated synthesis with negligible agglomeration. Conversely, **Figure 15 (b)**, following dye adsorption, exhibits a rise in the range of 30 nm to 70 nm with an average size of 48 nm, with the particles growing larger and more agglomerated. This indicates that the dye molecules have attached to the nanoparticle surface, resulting in their aggregation. Notwithstanding this, the nanoparticles maintain their spherical morphology, exhibiting minor surface roughness. This comparison underscores the influence of dye adsorption on the dimensions and distribution of nanoparticles.

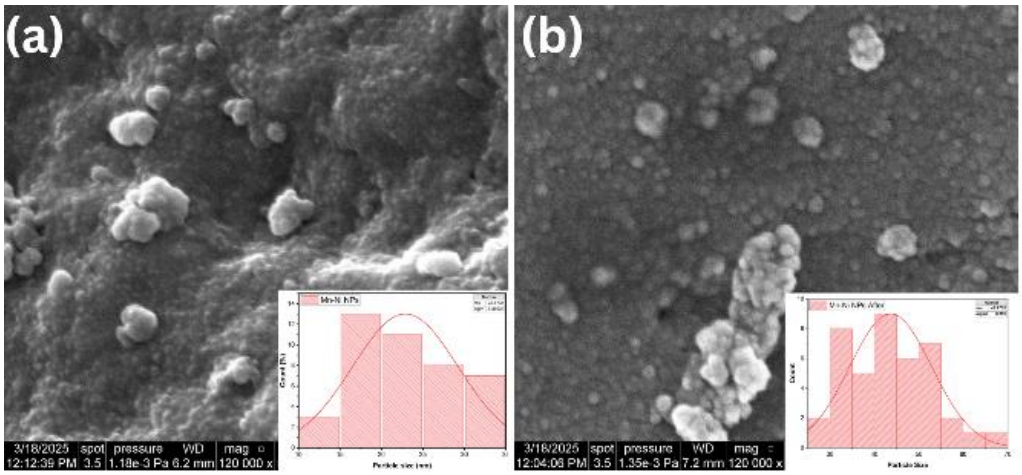

Figure 15: FE-SEM images of Mn-Ni nanoparticles, (a) before adsorption, (b) after adsorption.

4 Conclusion

This research presents an effective green synthesis of Ni and Mn–Ni bimetallic nanoparticles utilising Vigna unguiculata seed extract, providing an ecofriendly approach for removal of Congo Red dye from aqueous solutions. The synthesis process is characterised by minimal chemical reagent usage, brief calcination duration, and low metal

precursor concentration, which enhance its sustainability and cost-effectiveness. The bimetallic nanoparticles demonstrated a smaller average particle size (22 nm) relative to pure Ni (30 nm), leading to improved adsorption performance under optimised conditions 25 °C, 8 mg·L^{-1} dye concentration, 0.005 g catalyst dose, pH 7, and contact time 60 min. The adsorption behaviour was fitted well with Freundlich isotherm model and followed the pseudo second order kinetic, which indicate that the process is spontaneous and happened with exothermic nature. Moreover, the Mn–Ni nanoparticles was showed more stability in reusability and keep higher adsorption efficiency after three times using, in comparing to the monometallic Ni nanoparticles.

Acknowledgements

The authors are expressing their thankful to “Duhok Polytechnic University” and ”University of Zakho”, for their valuable supports and encouragements to complete the current research work.

Funding

This research received no external funding.

Authors contribution

LLM Conceptualization, Data curation, Analysis and Validation, Formal analysis, Investigation, Methodology, Resources, Software, Validation, Visualization, Writing original draft, **AKQ** Supervision, Methodology, Review and Editing.

Conflict of interests

The authors declare no conflicts of interest.

References

[1] K. Maheshwari, M. Agrawal, and A. B. Gupta, “Dye Pollution in Water and Wastewater,” 2021, 1–25. doi: 10.1007/978-981-16-2892-4_1.

[2] A. K. Qasim, “Novel Synthesis of Gold Doped Silver Phosphate Nanoparticles by Hydrothermal Method for The Enhancement of Visible Light-Responsive Photocatalytic Degradation of Fast Green FCF Dye,” *Science Journal of University of Zakho*, **10**(3), 76–80, doi: 10.25271/sjuoz.2022.10.3.916 (Jul. 2022).

[3] S. I. Siddiqui *et al.*, “Investigation of Congo Red Toxicity towards Different Living Organisms: A Review,” *Processes*, **11**(3), 807, doi: 10.3390/pr11030807 (Mar. 2023).

[4] M. Berradi *et al.*, “Textile finishing dyes and their impact on aquatic environs,” *Heliyon*, **5**(11), e02711, doi: 10.1016/j.heliyon.2019.e02711 (Nov. 2019).

[5] T. S. Vo, M. M. Hossain, T. Lim, J. W. Suk, S. Choi, and K. Kim, “Modification of the interfacial glass fiber surface through graphene oxide-3 chitosan interactions for excellent dye removal as an adsorptive membrane Modification of the interfacial glass fiber surface through graphene oxide-23 chitosan interactions for excellent dye removal as an adsorptive membrane.” [Online]. Available: https://ssrn.com/abstract=4156669

[6] X. Yao, P. Huang, and Z. Nie, “Cyclodextrin-based polymer materials: From controlled synthesis to applications,” *Prog Polym Sci*, **93**, 1–35, doi: 10.1016/j.progpolymsci.2019.03.004 (Jun. 2019).

[7] H. Agarwal, S. Venkat Kumar, and S. Rajeshkumar, “A review on green synthesis of zinc oxide nanoparticles – An eco-friendly approach,” *Resource-Efficient Technologies*, **3**(4), 406–413, doi: 10.1016/j.reffit.2017.03.002 (Dec. 2017).

[8] P. Singh, Y.-J. Kim, D. Zhang, and D.-C. Yang, “Biological Synthesis of Nanoparticles from Plants and Microorganisms,” *Trends Biotechnol*, **34**(7), 588–599, doi: 10.1016/j.tibtech.2016.02.006 (Jul. 2016).

[9] J. Singh, T. Dutta, K.-H. Kim, M. Rawat, P. Samddar, and P. Kumar, “‘Green’ synthesis of metals and their oxide nanoparticles: applications for environmental remediation,” *J Nanobiotechnology*, **16**(1), 84, doi: 10.1186/s12951-018-0408-4 (Dec. 2018).

[10] E. N. Yonan, N. M. Sher Mohammed, and A. K. Qasim, “Green synthesis and characterisation of monometallic (Ni) and bimetallic (Ni-Ag) nanoparticles using Cicer Arietinum leaf extract and their applications for adsorption of toluidine blue,” *Int J Environ Anal Chem*, 2022, doi: 10.1080/03067319.2022.2118594.

[11] A. Chatterjee, J. Abraham, M. Ajantha, A. Talekar, and N. Revathy, “Biosynthesis, Antimicrobial and Cytotoxic Effects of Titanium Dioxide Nanoparticles Using Vigna unguiculata Seeds,” *International Journal of Pharmacognosy and Phytochemical Research*, **9**, 95–99, , doi: 10.25258/ijpapr.v9i1.8047 (Jan. 2017).

[12] I. Khan, K. Saeed, and I. Khan, “Nanoparticles: Properties, applications and toxicities,” Nov. 01, 2019, *Elsevier B.V.* doi: 10.1016/j.arabjc.2017.05.011.

[13] L. L. Mustafa and A. K. Qasim, "Facile green synthesis of Mn doped NiO nanoparticles using Vigna unguiculata seed for photocatalytic degradation of toluidine blue," *Int J Environ Anal Chem*, doi: 10.1080/03067319.2025.2487850 (2025).
[14] L. Y. Mohammed, "ANTIOXIDANT ACTIVITY AND PHYSICO-CHEMICAL PROPERTIES OF GREEN SYNTHESIZED ZINC OXIDE NANOPARTICLES USING ERUCA SATIVA LEAF EXTRACT," *Science Journal of University of Zakho*, **11**(4), doi: 10.25271/sjuoz.2023.11.4.1173 (Dec. 2023).
[15] A. A. Goyi, N. M. Sher Mohammad, and K. M. Omer, "Preparation and characterization of potato peel derived hydrochar and its application for removal of Congo red: a comparative study with potato peel powder," *International Journal of Environmental Science and Technology*, **21**(1), 631–642, doi: 10.1007/s13762-023-04965-y (Jan. 2024).
[16] I. Aminu, S. M. Gumel, W. A. Ahmad, and A. A. Idris, "Adsorption Isotherms and Kinetic Studies of Congo-Red Removal from Waste Water Using Activated Carbon Prepared from Jujube Seed," *Am J Analyt Chem*, **11**(01), 47–59, doi: 10.4236/ajac.2020.111004 (2020).
[17] R. Lafi, I. Montasser, and A. Hafiane, "Adsorption of congo red dye from aqueous solutions by prepared activated carbon with oxygen-containing functional groups and its regeneration," *Adsorption Science and Technology*, **37**, (1–2), 160–181, doi: 10.1177/0263617418819227 (Mar. 2019).
[18] A. Pratt, "Environmental applications of magnetic nanoparticles," in *Frontiers of Nanoscience*, **6**, Elsevier Ltd, 2014, 259–307. doi: 10.1016/B978-0-08-098353-0.00007-5.
[19] A. A. Goyi, N. M. Sher Mohammad, and K. M. Omer, "Nitrogen-rich, potato peel-derived hydrochar as an effective dye adsorbent," *Biofuels*, doi: 10.1080/17597269.2024.2336323 (2024).
[20] A. Bavi, M. S. Jafari, M. Heydari, F. Ebrahimi, and A. Sadeghizadeh, "Batch and continuous mode adsorption of methylene blue cationic dye onto synthesized titanium dioxide/polyurethane nanocomposite modified by sodium dodecyl sulfate," *Colloids and Surfaces C: Environmental Aspects*, **1**, 100012, doi: 10.1016/j.colsuc.2023.100012 (Nov. 2023).
[21] R. Islam *et al.*, "Modulating Mn-doped NiO nanoparticles: structural, optical, and electrical property tailoring for enhanced hole transport layers," *Nanoscale Adv*, doi: 10.1039/d4na00708e (Oct. 2024).
[22] V. A. Mane, D. V. Dake, N. D. Raskar, R. B. Sonpir, M. D. Shirsat, and B. N. Dole, "Optimization, kinetic analysis, and photocatalytic degradation of rhodamine B using manganese doped nanoscale nickel oxide nanoparticles," *Ceram Int*, **50**(20), 38871–38883, doi: 10.1016/j.ceramint.2024.07.250 (Oct. 2024).
[23] F. Taghizadeh, "The Study of Structural and Magnetic Properties of NiO Nanoparticles," *Optics and Photonics Journal*, **06**(08), 164–169, doi: 10.4236/opj.2016.68b027(2016).
[24] K. H. J. Buschow, P. G. Van Engen, and R. Jongebreur, "MAGNETO-OPTICAL PROPERTIES OF METALLIC FERROMAGNETIC MATERIALS," 1983.
[25] U. Ahmed, D. Sundholm, and M. P. Johansson, "The effect of hydrogen bonding on the π depletion and the π-π stacking interaction," *Physical Chemistry Chemical Physics*, **26**(43), 27431–27438, doi: 10.1039/d4cp02889a (Oct. 2024).
[26] K. R. Ahmed, D. S. Mohammed, and F. M. Ali, "SYNTHESIS OF A NEW ADSORBENT BASED ON THE MILD DEALUMINATED BINDER FREE GRANULAR Y ZEOLITE," *Science Journal of University of Zakho*, **11**(3), doi: 10.25271/sjuoz.2023.11.3.1115 (Jul. 2023).
[27] P. Palai, S. Muduli, B. Priyadarshini, and T. R. Sahoo, "A facile green synthesis of ZnO nanoparticles and its adsorptive removal of Congo red dye from aqueous solution," in *Materials Today: Proceedings*, Elsevier Ltd, 2020, 2445–2451. doi: 10.1016/j.matpr.2020.07.387.
[28] I. Ali, Z. A. AL-Othman, and A. Alwarthan, "Molecular uptake of congo red dye from water on iron composite nano particles," *J Mol Liq*, **224**, 171–176, doi: 10.1016/j.molliq.2016.09.108 (Dec. 2016).
[29] H. Zhu, W. Wang, Y. Huo, X. He, H. Zhao, and H. Wang, "Molecular Simulation Study on Adsorption and Diffusion Behaviors of CO2/N2in Lignite," *ACS Omega*, **5**(45), 29416–29426, doi: 10.1021/acsomega.0c04352 (Nov. 2020).
[30] X. Yang, X. Cao, C. Chen, L. Liao, S. Yuan, and S. Huang, "Green Synthesis of Zinc Oxide Nanoparticles Using Aqueous Extracts of Hibiscus cannabinus L.: Wastewater Purification and Antibacterial Activity," *Separations*, **10**(9), doi: 10.3390/separations10090466 (Sep. 2023).